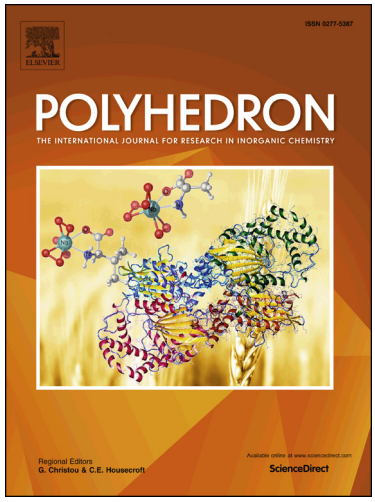

In-situ IR Monitoring to Probe the Formation of Structural Defects in Zr-fumarate Metal-organic Framework (MOF)

Jianwei Ren, Nicholas M. Musyoka, Henrietta W. Langmi, Joseph Walker, Mkhulu Mathe, Shijun Liao

PII: S0277-5387(18)30413-3
DOI: https://doi.org/10.1016/j.poly.2018.07.026
Reference: POLY 13291

To appear in: *Polyhedron*

Received Date: 27 March 2018
Revised Date: 7 June 2018
Accepted Date: 16 July 2018

Please cite this article as: J. Ren, N.M. Musyoka, H.W. Langmi, J. Walker, M. Mathe, S. Liao, In-situ IR Monitoring to Probe the Formation of Structural Defects in Zr-fumarate Metal-organic Framework (MOF), *Polyhedron* (2018), doi: https://doi.org/10.1016/j.poly.2018.07.026

In-situ IR Monitoring to Probe the Formation of Structural Defects in Zr-fumarate Metal-organic Framework (MOF)

Jianwei Ren[a,b]*, Nicholas M. Musyoka[a], Henrietta W. Langmi[a], Joseph Walker[c], Mkhulu Mathe[a], Shijun Liao[d]

[a]Energy Centre, Council for Scientific and Industrial Research (CSIR), Meiring Naudé Road, Brummeria, Pretoria 0001, South Africa.

[b]Mechanical Engineering Science Department, University of Johannesburg, Johannesburg, South Africa.

[c]Resolution Circle Pty. Ltd., Johannesburg, South Africa.

[d]School of Chemistry and Chemical Engineering, South China University of Technology, Wushan Road, Tianhe district, Guangzhou 510640, China.

E-mail: jren@csir.co.za; Tel: +27 (0)12 841 2967

Abstract

In this work, in-situ IR monitoring technique was employed to monitor the crystallization process of Zr-fumarate (Zr-fum) MOF in both H_2O- and DMF-based systems. Wherein, the acid modulator (HCOOH) was only observed to be consumed in the DMF-based synthesis. Further solid-state NMR ex-situ results suggested the participations of HCOOH in the Zr-fum MOF structure formation, resulting in the possibility of formation of structural defects. This observation will further help to understand the formation of MOF structural defects from different solvent systems.

Keywords: Structural defects; Zr-fumarate MOF; In-situ IR monitoring; Solvent-dependent

1. Introduction

'Defects engineering' in metal-organic frameworks (MOFs) has been proposed to be an important strategy during the shaping of their physical/chemical behaviors such as stability [1,2], sorption [3,4], catalytic behavior [5], proton conductivity [6], acidity [7], ferromagnetism [8] and thermal expansion [9,10]. Usually, the straightforward routes of combining metal ions with organic linkers often result in a MOF with deviations from its ideal crystal orderliness [11]. If no other changes are conducted during the synthesis process, except mixing of the usual building blocks of the parent framework under conventional synthetic conditions, the ensuing MOFs are reported to be susceptible to displaying ''inherent defects" [10]. These defects originate either from misconnections or dislocations that happen during the crystallization process or from post-crystallization modifications [10]. Among several other well-known defect creation strategies [1–6], modulation synthesis strategy that had been introduced by Kitagawa group [12,13] with the prior intention of improving the crystallinity and reproducibility of MOFs synthesis has been reported to induce defects into MOF structures [14]. These defects have been reported to exhibit strong dependence on the nature of the modulator acid used [15,16]. Even though a number of ex-situ detection techniques such as single-crystal X-ray diffraction (SXRD), surface area analysis, thermogravimetric analysis (TGA), IR spectroscopy analysis,

atomic force microscopy [17–21] and Raman spectrum [22] have been used to detect the formation of MOF structural defects, to date, the answer to the question of whether and how the acid modulator would participate in the formation of MOF structure is still based on assumptions [23–27]. To enable 'defects engineering' towards the properties of interest, further understanding of the formation processes of MOF defects is warranted. Earlier studies on the synthesis of Zr-fumarate (Zr-fum) MOF, with the empirical formula of $Zr_6O_4(OH)_4(C_4O_4)_6$, have revealed that this MOF could be synthesized either from water- or N,N-dimethylformamide (DMF)-based reaction systems [28–32]. From our previous work [33,34], we had observed that the addition of formic acid to the DMF-based reaction system led to the formation of the seeding crystals with different shapes compared to water-based synthesis, and this allowed us to assume that the formation mechanisms of Zr-fum MOF from the two different solvent systems can be different. In other words, the way the acid modulator participates in the formation process of Zr-fum MOFs structure can also be different.

In this work, in-situ IR monitoring technique (Fig. S1) was employed, under real synthesis conditions, to monitor the crystallization of Zr-fum MOF in both water- and DMF-based modulated synthesis systems. In addition, the obtained Zr-fum MOF samples were further characterized using ex-situ techniques including X-ray diffraction (XRD), focused-ion beam scanning electron microscope (FIB-SEM), Fourier transform infrared (FTIR) spectroscopy, solid-state ^{13}C nuclear magnetic resonance (NMR), and surface area and pore characteristics measurements so as to complement the in-situ studies.

2. Experimental Section

2.1. Reagents and Chemicals

Zirconium tetrachloride ($ZrCl_4$, Sigma–Aldrich, 99.5+%), fumaric acid ($C_4H_4O_4$, Sigma–Aldrich, 99+%), N,N-dimethylformamide (DMF, Sigma-Aldrich, 99.8%) and formic acid (HCOOH, Sigma–Aldrich, 95+%) were purchased and used without further purification. De-ionized water was obtained from a water purification system (Instrubal, Zeneer Power II) in the laboratory.

2.2. In-situ IR monitoring synthesis of Zr-fum MOF from both H_2O- and DMF-based systems

Experiments were conducted on a combined in-situ IR reaction system (EasyMax 102/ReactorIR™ 15), and the programmes were executed on ICONTROL-PC running IControl version 5.4.217.0. The IR data was obtained using iC IR™ reaction analysis software. There were two concurrent reactions that were carried out as shown in Fig. S1. The left reactor was run as a reference while the right reactor was for IR recording. The experimental procedure was split into five phases: Phase I, initial solution of $ZrCl_4/H_2O$ was added and a waiting time of 5 min allowed while recording IR data; Phase II, formic acid was added and IR data collected for another 5 min; Phase III, fumaric acid/H_2O solution was added and IR information collected for an additional 5 min; Phase IV, heating at 10 °C/min up to 80 °C was started and held for 1200 min whilst collecting the IR data; Phase V, the system was cooled to 25 °C at 5 °C/min while still collecting the IR data. During the reaction, the product from the left reactor was sampled at specific time intervals for further tests. After the reaction was terminated, the resulting white precipitate was washed with water/ethanol, collected by centrifugation and dried at

100 °C for 24 h. For comparison purpose, Zr-fum MOF crystals were also synthesized from DMF-based system still following the above mentioned in-situ monitoring procedure but replacing H_2O with DMF as a solvent.

2.3. Characterization

X-ray diffraction (XRD) patterns were obtained at room temperature by using a PANalytical X'Pert Pro powder diffractometer with Pixcel detector using Ni-filtered Cu-K_α radiation (0.154 nm) in the range of 2θ = 1–50°, and scanning rate of 0.1 °·s^{-1}. An Auriga Cobra Focused-Ion Beam Scanning Electron Microscope (FIB-SEM) was used to study the morphology of the obtained Zr-fum MOF samples. All the samples were mounted on a carbon tape and coated with gold prior to measurement. Fourier transform infrared (FTIR) spectroscopy was scanned at 4 cm^{-1} resolution in the range of 400–4000 cm^{-1} on a Perkin Elmer Spectrum 400 FT-IR/FT-NIR Spectrometer. Solid state NMR experiments were carried out using 2.5 mm outer diameter zirconia rotors (Bruker, Karlsruhe, Germany). ^{13}C NMR spectra were obtained with a Bruker AVANCE III HD 500 MHz (11.1 Tesla) standard bore spectrometer and triple channel broad band probe (TrigammaTM MAS probe), at a magic angle spinning rate of 20 kHz, frequencies of 500 MHz (1H) and 125.8 MHz (13C) and standard cross polarization (CP) MAS techniques (1H π/2 pulse length 2.2 s, 1H cross polarization field 120 kHz, 1H–13C cross polarization contact time 2.0 ms, broadband SPINAL64 decoupling during signal acquisition at a 1H field strength of 120 kHz, recycle time 5 s, and typical number of scans accumulated per spectrum ca. 3000). Chemical shifts were referenced to the downfield methylene signal from solid adamantane at 38.3 ppm. Surface area and pore characteristics measurements were carried out on an ASAP 2020 HD analyzer (Micromeritics) using N_2. Hydrogen adsorption isotherms at 77 K and pressure up to 1 bar were also measured on the ASAP 2020 instrument. All gas sorption isotherms were obtained using ultra-high purity grade (99.999%) gases. Considering that the as-prepared MOF samples may contain some carboxylic acid impurities within the pores, before analysis, MOF samples (0.2–0.3 g) were first solvent-exchanged using ethanol and pre-treated in an oven. Then the samples were outgassed in the analysis tube under vacuum (down to 10^{-7} bar) with heating up to 200 °C, which is sufficient to remove impurities without causing thermal decomposition or loss of framework crystallinity. In addition, the pH change from the reaction systems were also monitored by the equipped pH probes, as shown in Fig. S1.

3. Results and discussion

The XRD patterns of the resulting Zr-fum MOF samples are shown in Fig. 1a. The characteristic reflection signals fit well with the simulated pattern and also the experimental patterns reported earlier [28, 35] and thus confirming the successful synthesis of Zr-fum MOF from both H_2O- and DMF-based systems. The 'broad peak' in the 2θ range of 3–7° for both XRD patterns indicate the missing cluster defects in the two Zr-fum MOF samples [36]. Noteworthy, the relatively higher intensity of this peak for the Zr-fum MOF sample derived from DMF-based system suggests the higher concentration of the missing cluster defects. In the FTIR spectra (Fig. 1b), the peak at 1399 cm^{-1} corresponds to C-C stretching from the fumaric acid linker for the two Zr-fum MOFs samples. It was noted that the peak at

1102 cm^{-1}, for the Zr-fum sample derived from DMF-based system, corresponds to C-O stretches that might arise from modulator (HCOOH) and acid linker (fumaric acid). The signal at 1659 cm^{-1}, that was assigned to C=O stretches, may be ascribed to the participation of formic acid (HCOOH), acid linker (fumaric acid) or solvent (DMF) in the formation of the MOF structure. Since the signals at 1102 cm^{-1} and 1659 cm^{-1} are absent for the Zr-fum sample derived from H_2O-based system, it is possible that the modulator (HCOOH) was incorporated into the network structure of Zr-fum MOF and thus creating connectivity defects in the structure. The N_2 adsorption isotherms in Fig. 1c indicate that the BET surface area and porosity of Zr-fum MOF sample derived from DMF-based system is higher than that derived from H_2O-based system. In Fig. 1d, the deviations of the pore sizes from the expected range (5–7 Å) for the two Zr-fum samples are observed [28], which could be as a result of the presence of structural defects [37–39]. The pore size for Zr-fum MOF sample derived from DMF-based system shifted further towards larger pore width, which further suggests that the Zr-fum MOF sample from the DMF-based system contains more missing cluster defects than the Zr-fum MOF sample obtained from the H_2O-based system. Fig. 1e and 1f show the differences in morphology of the parent Zr-fum MOFs derived from the two different solvent systems. In the H_2O-based system, the obtained Zr-fum MOFs morphology was 'soccer ball'-like whereas that from the DMF-based system had the octahedral shapes.

Fig. 2 shows the 3D plot of FTIR spectra collected over time under H_2O-based reaction system. The addition of $ZrCl_4$ to water (Phase I, Fig. 2a) caused a spike in the intensity of peaks positioned at 671 cm^{-1} and 1630 cm^{-1}. As indicated by the equipped pH probes (Fig. S1), this anomaly could be due to the hydrolysis of the $ZrCl_4$ precursor, which was observed to lead to a dramatic decrease of the pH value to below 1 due to the formation of hydrochloric acid. Similar observations were also reported by Zahn et al. [40]. Upon addition of formic acid, three new peaks (1719, 1405 and 1244 cm^{-1}) associated with formic acid were observed in Fig. 2b (Phase II). The failure to obtain other peaks that had been observed for pristine formic acid (671, 812, and 1172 cm^{-1}; Fig. S3) could be due to the complex chemistry that happened due to interactions with the newly formed species from the hydrolysis of the Zr salt. After the addition of fumaric acid/H_2O solution, the increased intensities of IR peaks positioned at 1719, 1405 and 1244 cm^{-1} were observed in Fig. 2c (Phase III) and may be due to the transformation of fumaric acid into malic acid in the presence of water and high temperatures [41].

From the 3D plots of FTIR spectra at different phases and also from the recorded IR peaks in Table S1, several new peaks positioned at 670, 983 and 1585 cm^{-1} were found to start appearing just a few minutes after the onset of heating (Phase IV, Fig. 2d) and gradually increased to a plateau after 1 h (Fig. 2e). This observation corresponded to the formation of Zr-fum MOF. The lack of further intensity changes for peaks in Fig. 2e that had been associated with formic acid served to indicate that formic acid acted as a 'deprotonation modulator', which is an observation that has been generally known from earlier work [42,43]. In this case, the involvement of the carboxyl group of the modulator (formic acid) would initially start during the formation of clusters with the metal cations and thus modulate the MOF crystallization process. In other words, the formic acid in the H_2O-based system only facilitated

the attachment of the linker molecules to the inorganic building units (IBUs) of Zr-fum MOF and hence agreeing with one of the reported proposals of modulation mechanisms [44].

In the DMF-based system, consumption of formic acid was accompanied by the corresponding peak height changes that were observed in Fig. 3e (pointed out by red arrows) when formic acid was added into the $ZrCl_4$/DMF solution. This observation served to indicate that formic acid participated in the structure formation of Zr-fum MOF crystals. As observed from Fig. 3b and Table S1, the signals at 1172 cm^{-1} and 1670 cm^{-1} in Fig. 3e are from the contribution of formic acid whereas signals at 1091 cm^{-1} and 1253 cm^{-1} can be attributed to DMF. The other signal assignments can also be seen in Fig. 3e. In this case, it is suggested that the initial Zr-fum MOF nuclei were generated during the initial stages of the crystallization process when the formic acid reacted with $ZrCl_4$, which agrees well with the visual observation that the addition of formic acid to the synthesis mixture induced the quicker formation of the seeding crystals. The dramatic drop of the two corresponding peak heights for formic acid observed after the addition of formic acid provides evidence to the earlier formulated hypothesis that acid-modulated reaction might start with the fast formation of the soluble discrete modulator-capped Zr_6 clusters [45]. Through reversible ligand exchange with the ditopic linker acid, the final 3D structure is formed by the assembly of these clusters. It is also notable that during the formation of Zr-fum MOF, the heights of the DMF peaks in Fig. 3e also changed (pointed out by blue arrows). As a reaction solvent, such loss of DMF however could not be measured and apportioned to determine whether DMF was also consumed by forming the Zr-fum MOF structure or whether the IR peak reduction was caused by other reasons, i.e. simply pore-filling of Zr-fum MOF by DMF or chemical breakdown of DMF as suggested by Behrens [28], etc. The effect of the solvent may be due to the changes in the system polarization and the ability to preferentially solvate and thereby stabilize certain species in the acid-base equilibrium. In this case, water stabilizes the ionized species to a greater extent than does DMF.

Being a well-known analytical technique, solid-state NMR has been recognized as a vital method for assessing the incorporation of desired linkers or specific structural groups into the MOF lattice [46–50]. Considering the unescapable nature of defects in MOFs obtained from a modulation synthesis approach, NMR may be useful in identifying the point defects that are usually associated with either organic linkers or modulator acid. Trickett et al. [51] pointed out that the missing linker defects in UiO-66 could be due to water molecules that are coordinated directly to the Zr metal centers. During MOF crystallization the exchange of coordinated solvents from water to DMF has been reported [52]. The solid-state NMR results presented in Fig. 4, show signals assigned to HCOOH (peak 3) and DMF (peak 4, 5) for the Zr-fum MOF sample derived from the DMF-based system (Fig. 4b), and this may support the proposition that some of the DMF solvent was still present in the pore structure of Zr-fum MOF. Meanwhile the Zr-fum MOF sample derived from the H_2O-based system did not show these signals (Fig. 4a). This finding could possibly explain the earlier observation of consumption of formic acid and pore filling by DMF from in-situ monitoring DMF-based reaction system, as evidenced by the peak height changes in the 3D IR spectra. The peaks designated as 6 and 7 in Fig. 4b can be assigned to possibly dangling CH_2 groups from HCOOH modulator and BDC linker [53–55].

4. Conclusions

In summary, we have employed in-situ IR monitoring technique to monitor the crystallization process of Zr-fum MOF in both H_2O- and DMF-based systems. From DMF-based system, acid modulator (HCOOH) was observed to be consumed according to the recorded IR spectra and evidenced by the corresponding peak height changes, while the H_2O-based system showed otherwise. This observation serves to confirm the participation of formic acid during the structure formation of Zr-fum MOF derived from the DMF-based system. Further solid-state NMR results suggested the participations of HCOOH in the structure formation of Zr-fum MOF derived from DMF-based system, resulting in the formation of structural defects. The findings from this study will contribute to the further understanding of the formation of MOF structural defects in different solvent systems.

Acknowledgements

The authors acknowledge the financial supports from the South African Department of Science and Technology (DST) towards HySA Programme grant (EIMH01X), National Science Foundation (NRF) under the South Africa/France joint collaboration grant (EIMH06X) and DST-NRF Professional Development Programme grant (EIMH08X).

References

[1] A.W. Thornton, R. Babarao, A. Jain, F. Trousseletn, F.X. Coudert, “Defects in metal-organic frameworks: A compromise between adsorption and stability? Dalton Trans. 45 (2016) 4352–4359.

[2] S.J. Lee, C. Doussot, A. Baux, L. Liu, G.B. Jameson, C. Richardson, J.J. Pak, F. Trousselet, F.X. Coudert, S.G. Telfer, Multicomponent Metal-Organic Frameworks as Defect-Tolerant Materials, Chem. Mater. 28 (2016) 368–375.

[3] G.E. Cmarik, M. Kim, S.M. Cohen, K.S. Walton, Tuning the adsorption properties of UiO-66 via ligand functionalization, Langmuir 28 (2012) 15606–15613.

[4] B. Li, X.Y. Zhu, Y.S. Li, J.F. Feng, J.L. Shi, J.L. Gu, Defect creation in metal-organic frameworks for rapid and controllable decontamination of roxarsone from aqueous solution, J. Hazard. Mater. 302 (2016) 57–64.

[5] T.H. Park, A.J. Hickman, K. Koh, S. Martin, A.G. Wong-Foy, M.S. Sanford, A.J. Matzger, Highly dispersed palladium(II) in a defective metal-organic framework: application to C-H activation and functionalization, J. Am. Chem. Soc. 133 (2011) 20138–20141.

[6] J.M. Taylor, S. Dekura, R. Ikeda, H. Kitagawa, Defect Control To Enhance Proton Conductivity in a Metal–Organic Framework, Chem. Mater. 27 (2015) 2286–2289.

[7] J.M. Taylor, T. Komatsu, S. Dekura, K. Otsubo, M. Takata, H. Kitagawa, The role of a three dimensional ordered defect sublattice on the acidity of a sulfonated metal-organic framework, J. Am. Chem. Soc. 137 (2015) 11498–11506.

[8] L. Shen, S.W. Yang, S.C. Xiang, T. Liu, B.C. Zhao, M.F. Ng, J. Göettlicher, J.B. Yi, S. Li, L. Wang, J. Ding, B.L. Chen, S.H. Wei, Y.P. Feng, Origin of long-range ferromagnetic ordering

in metal–organic frameworks with antiferromagnetic dimeric-Cu(II) building units, J. Am. Chem. Soc. 134 (2012) 17286–17290.

[9] G.M. Psofogiannakis, G.E. Froudakis, Theoretical explanation of hydrogen spillover in metal-organic frameworks, J. Phys. Chem. C. 115 (2011) 4047–4053.

[10] M.J. Cliffe, J.A. Hill, C.A. Murray, F.X. Coudert, A.L. Goodwin, Defect-dependent colossal negative thermal expansion in UiO-66(Hf) metal–organic framework, Phys. Chem. Chem. Phys. 17 (2015) 11586–11592.

[11] D.S. Sholl, R.P. Lively, Defects in metal-organic frameworks: challenge or opportunity? J. Phys. Chem. Lett. 6 (2015) 3437–3444.

[12] T. Tsuruoka, S. Furukawa, Y. Takashima, K. Yoshida, S. Isoda, S. Kitagawa, Nanoporous nanorods fabricated by coordination modulation and oriented attachment growth, Angew. Chem. Int. Ed. 48 (2009) 4739–4743.

[13] S. Diring, S. Furukawa, Y. Takashima, T. Tsuruoka, S. Kitagawa, Controlled multiscale synthesis of porous coordination polymer in nano/micro regimes, Chem. Mater. 22 (2010) 4531–4538.

[14] F. Vermoortele, B. Bueken, G.L. Bars, B. Van de Voorde, M. Vandichel, K. Houthoofd, A. Vimont, M. Daturi, M. Waroquier, V. Van Speybroeck, C. Kirschhock, D.E. De. Vos, Synthesis modulation as a tool to increase the catalytic activity of metal-organic frameworks: the unique case of UiO-66(Zr), J. Am. Chem. Soc. 135 (2013) 11465−11468.

[15] O.V. Gutov, M.G. Hevia, E.C. Escudero-Adán, A. Shafir, Metal-organic framework (MOF) defects under control: insights into the missing linker sites and their implication in the reactivity of zirconium-based frameworks, Inorg. Chem. 54 (2015) 8396−8400.

[16] G.C. Shearer, S. Chavan, J. Ethiraj, J.G. Vitillo, S. Svelle, U. Olsbye, C. Lamberti, S. Boriga, K.P. Lillerud, Tuned to perfection: ironing out the defects in metal-organic framework UiO-66, Chem. Mater. 26 (2014) 4068−4071.

[17] M. Kandiah, M.H. Nilsen, S. Usseglio, S. Jakobsen, U. Olsbye, M. Tilset, C. Larabi, E.A. Quadrelli, F. Bonino, K.P. Lillerud, Synthesis and stability of tagged UiO-66 Zr-MOFs, Chem. Mater. 22 (2010) 6632−6640.

[18] P.S. Petkov, G.N. Vayssilov, J.X. Liu, O. Shekhah, Y.M. Wang, C. Wöll, T. Heine, Defects in MOFs: a thorough characterization, ChemPhysChem 13 (2012) 2025−2029.

[19] L. Valenzano, B. Civalleri, S. Chavan, S. Bordiga, M.H. Nilsen, S. Jakobsen, K.P. Lillerud, C. Lamberti, Disclosing the complex structure of UiO-66 metal-organic framework: a synergic combination of experiment and theory, Chem. Mater. 23 (2011) 1700−1718.

[20] M. Shöâeè, J.R. Agger, M.W. Anderson, M.P. Attfield, Crystal form, defects and growth of the metal-organic framework HKUST-1 revealed by atomic force microscopy, CrystEngComm 10 (2008) 646−648.

[21] S. Øien, D. Wragg, H. Reinsch, S. Svelle, S. Bordiga, C. Lamberti, K.P. Lillerud, Detailed structure analysis of atomic positions and defects in zirconium metal-organic frameworks, Cryst. Growth Des. 14 (2014) 5370−5372.

[22] J.W. Ren, H.W. Langmi, N.M. Musyoka, M. Mathe, X.D. Kang, Tuning defects to facilitate hydrogen storage in core-shell MIL-101(Cr)@UiO-66(Zr) nanocrystals, Materials Today: Proceedings 2 (2015) 3964−3972.

[23] Z.L. Fang, B. Bueken, D.E. De Vos, R.A. Fischer, Defect-engineered metal-organic frameworks, Angew. Chem. Int. Ed. 54 (2015) 7234−7254.

[24] O. Kozachuk, I. Luz, F.X. Llabrési Xamena, H. Noei, M. Kauer, H.B. Albada, E.D. Bloch, B. Marler, Y.M. Wang, M. Muhler, R.A. Fischer, Multifunctional, defect-engineered metal-organic frameworks with ruthenium centers: sorption and catalytic properties, Angew. Chem. Int. Ed. 53 (2014) 7058−7062.

[25] W.B. Liang, C.J. Coqhlan, F. Raqon, M. Rubio-Martinez, D.M. D'Alessandro, R. Babarao, Defect engineering of UiO-66 for CO_2 and H_2O uptake−a combined experimental and simulation study, Dalton Trans. 45 (2016) 4496−4500.

[26] Z.R. Jiang, H.W. Wang, Y.L. Hu, J.L. Lu, H.L. Jiang, Polar group and defect engineering in a metal-organic framework: synergistic promotion of carbon dioxide sorption and conversion, ChemSusChem 8 (2015) 878−885.

[27] T. Cheetham, T.D. Bennett, F.X. Coudert, A. Goodwin, Defects and disorder in metal organic frameworks, Dalton Trans. 45 (2016) 4113–4126.

[28] G. Wißmann, A. Schaate, S. Lilienthal, I. Bremer, A.M. Schnerder, P. Behrens, Modulated synthesis of Zr-fumarate MOF, Micropor. Mesopor. Mater. 152 (2012) 64−70.

[29] G. Zahn, H. A. Schulze, J. Lippke, S. König, U. Sazama, M. Fröba, P. Behrens, A water-born Zr-based porous coordination polymer: modulated synthesis of Zr-fumarate MOF, Micropor. Mesopor. Mater. 203 (2015)186−194.

[30] J.H. Luo, H. W. Xu, Y. Liu, Y.S. Zhao, L.L. Daemen, C. Brown, T.V. Timofeeva, S.Q. Ma, H.C. Zhou, Hydrogen adsorption in a highly stable porous rare-earth metal-organic framework: sorption properties and neutron diffraction studies, J. Am. Chem. Soc. 130 (2008) 9626−9627.

[31] G. Yushin, R. Dash, J. Jagiello, J.E. Fisher, Y. Gogotsi, Carbide-derived carbons: effect of pore size on hydrogen uptake and heat of adsorption, Adv. Funct. Mater. 16 (2006) 2288−2293.

[32] M. Ganesh, P. Hemalatha, M.M. Peng, W. S. Cha, H.T. Jang, Zr-fumarate MOF a novel CO_2-adsorbing material: synthesis and characterization, Aerosol Air Qual. Res. 14 (2014) 1605−1612.

[33] J.W. Ren, N.M. Musyoka, H.W. Langmi, B.C. North, M. Mathe, X.D. Kang, S.J. Liao, Hydrogen storage in Zr-fumarate MOF, Int. J. Hydrogen Energy, 40 (2015) 10542–10546.

[34] J.W. Ren, N.M. Musyoka, H.W. Langmi, M. Mathe, W. Pang, M.J. Wang, J. Walker, In-situ IR monitoring of the formation of Zr-fumarate MOF, App. Sur. Sci. 404 (2017) 263–267.

[35] H. Furukawa, F. Gándara, Y.B. Zhang, J.C. Jiang, W.L. Queen, M.R. Hudson, O.M. Yaghi, Water adsorption in porous metal-organic frameworks and related materials, J. Am. Chem. Soc. 136 (2014) 4369−4381.

[36] G.C. Shearer, S. Chavan, S. Bordiga, S. Svelle, U. Olsbye, K.P. Lillerud, Defect engineering: tuning the porosity and composition of the metal-organic framework UiO-66 via modulated synthesis. Chem. Mater. 28 (2016) 3749−3761.

[37] C.V. McGuire, R.S. Forgan, The surface chemistry of metal-organic frameworks, Chem. Commun. 51 (2015) 5199−5217.

[38] H. Wu, Y.S. Chua, V. Krungleviciute, M. Tyagi, P. Chen, T. Yildirim, W. Zhou, Unusual and Highly Tunable Missing-Linker Defects in Zirconium Metal–Organic Framework UiO-66 and Their Important Effects on Gas Adsorption, J. Am. Chem. Soc. 135 (2013) 10525−10532.

[39] B. Bueken, H. Reinsch, N. Reimer, I. Stassen, F. Vermoortele, R. Ameloot, N. Stock, C.E.A. Kirschhock, D. De Vos, A zirconium squarate metal–organic framework with modulator-dependent molecular sieving properties, Chem. Commun. 50 (2014) 10055−10058.

[40] G. Zahn, P. Zerner, J. Lippke, F.L. Kempf, S. Lilienthal, C.A. Schröder, A.M. Schneider, P. Behrens, Insight into the mechanism of modulated syntheses: in situ synchrotron diffraction studies on the formation of Zr-fumarate MOF, CrystEngComm. 16 (2014) 9198−9207.

[41] J. Rivas, S.T. Kolaczkowski, F. J. Beltran, D.B. McLurgh. Degradation of maleic acid in a wet air oxidation environment in the presence and absence of a platinum catalyst. Appl. Catal. B Environ. 22 (1999) 279−291.

[42] R. Ameloot, F. Vermoortele, J. Hofkens, F.C. De Scheyver, D.E. De Ves, M.B.J. Roeffaers, Three-Dimensional Visualization of Defects Formed during the Synthesis of Metal–Organic Frameworks: A Fluorescence Microscopy Study, Angew. Chem. Int. Ed. 52 (2013) 401−405.

[43] Z. Zhu, D. Zhao, De facto methodologies toward the synthesis and scale-up production of UiO-66-type metal-organic frameworks and membrane materials, Dalton Trans. 44 (2015) 19018−19040.

[44] Q.Y. Yang, A.D. Wiersum, H. Jobie, V. Guillerm, C. Serre, P.L. Llewellyn, G. Manrim, Understanding the Thermodynamic and Kinetic Behavior of the CO_2/CH_4 Gas Mixture within the Porous Zirconium Terephthalate UiO-66(Zr): A Joint Experimental and Modeling Approach, J. Phys. Chem. C 115 (2011) 13768−13774.

[45] F. Ragon, H. Chevreau, T. Devic, C. Serre, P. Horcajada, Impact of the Nature of the Organic Spacer on the Crystallization Kinetics of UiO-66(Zr)-Type MOFs, Chem. Eur. J. 21 (2015) 7135−7143.

[46] V. Guillerm, S. Gross, C. Serre, T. Devic, M. Bauer, G. Férey, A zirconium methacrylate oxocluster as precursor for the low-temperature synthesis of porous zirconium(IV) dicarboxylates, Chem. Commun. 46 (2010) 767−769.

[47] A. Sutrisno, Y. N. Huang, Solid-state NMR: A powerful tool for characterization of metal–organic frameworks, Solid State Nucl. Magn. Reson. 49-50 (2013) 1−11.

[48] Y.J. Jiang, J. Huang, B.B. Kasumaj, G. Jeschke, M. Hunger, T. Mallat, A. Baiker, Adsorption−Desorption Induced Structural Changes of Cu-MOF Evidenced by Solid State NMR and EPR Spectroscopy, J. Am. Chem. Soc. 131 (2009) 2058−2059.

[49] H.C. Hoffmann, M. Debowski, P. Müller, S. Paasch, I. Senkovska, S. Kaskel, E. Brunner, Solid-State NMR Spectroscopy of Metal–Organic Framework Compounds (MOFs), Materials 5 (2012) 2537−2572.

[50] F. Gul-E-Noor, B. Jee, A. Pöppl, M. Hartmann, D. Himsl, M. Bertmer, Effects of varying water adsorption on a $Cu_3(BTC)_2$ metal–organic framework (MOF) as studied by ^{1}H and ^{13}C solid-state NMR spectroscopy, Phys. Chem. Chem. Phys. 13 (2011) 7783−7788.

[51] C.A. Trickett, K.J. Gagnon, S. Lee, F. Gándara, H.B. Bürgi, O.M. Yaghi, Definitive Molecular Level Characterization of Defects in UiO-66 Crystals, Angew. Chem. 127 (2015) 11314−11319.

[52] Y. Wu, M.I. Breeze, G.J. Clarkson, F. Millange, D. O'Hare, R.I. Walton, Exchange of coordinated solvent during crystallization of a metal-organic framework observed by in situ high-energy X-ray diffraction, Angew. Chem. 128 (2016) 5076−5080.

[53] C.Y. Zhang, C. Hang, D.S. Sholl, J.R. Schmidt, Computational characterization of defects in metal-organic frameworks: spontaneous and water-induced point defects in ZIF-8, J. Phys. Chem. Lett. 7 (2016) 459−464.

[54] Y. Luan, Y. Qi, H.Y. Gao, R.S. Andriamitantsoa, N.N. Zheng, G. Wang, A general post-synthetic modification approach of amino-tagged metal–organic frameworks to access efficient catalysts for the Knoevenagel condensation reaction, J. Mater. Chem. A 3 (2015) 17320−17331.

[55] S. Henke, A. Schneemann, A. Wütscher, R. A. Fischer, Directing the Breathing Behavior of Pillared-Layered Metal–Organic Frameworks via a Systematic Library of Functionalized Linkers Bearing Flexible Substituents, J. Am. Chem. Soc. 134 (2012) 9464−9474.

Fig. 1. (a) XRD patterns, (b) FTIR spectra, (c) N_2 sorption isotherms, (d) pore size distribution, (e) SEM image of Zr-fum MOF sample from H_2O-based system, and (f) SEM image of Zr-fum MOF sample from DMF-based system.

Fig. 2. 3-dimensional plot of FTIR spectra collected over time showing the consumption of reactants and the appearance of the Zr-fum MOF product under H_2O-based system: (a) Phase I, $ZrCl_4/H_2O$ solution; (b) Phase II, add formic acid; (c) Phase III, add fumaric acid/H_2O solution; (d) Phase IV, heat up the reaction; and (e) the 60 min in-situ IR reaction.

Fig. 3. 3-dimensional plot of FTIR spectra collected over time showing the consumption of reactants and the appearance of the Zr-fum MOF product under DMF-based system: (a) Phase I, $ZrCl_4$/DMF solution; (b) Phase II, add formic acid; (c) Phase III, add fumaric acid/DMF solution; (d) Phase IV, heat up the reaction; and (e) the 60 min in-situ IR reaction.

Fig. 4. ^{13}C solid-state NMR spectra of Zr-fum MOF sample: (a) H_2O-based system, and (b) DMF-based system.

Highlights

1. In-situ IR monitoring technique was used to monitor the crystallization of Zr-fumarate MOF in both DMF-/H_2O-based systems.
2. The HCOOH and DMF were only observed participating into the MOF structural formation in DMF-based system.
3. The results will further help to understand the formation of structural defects in MOFs.

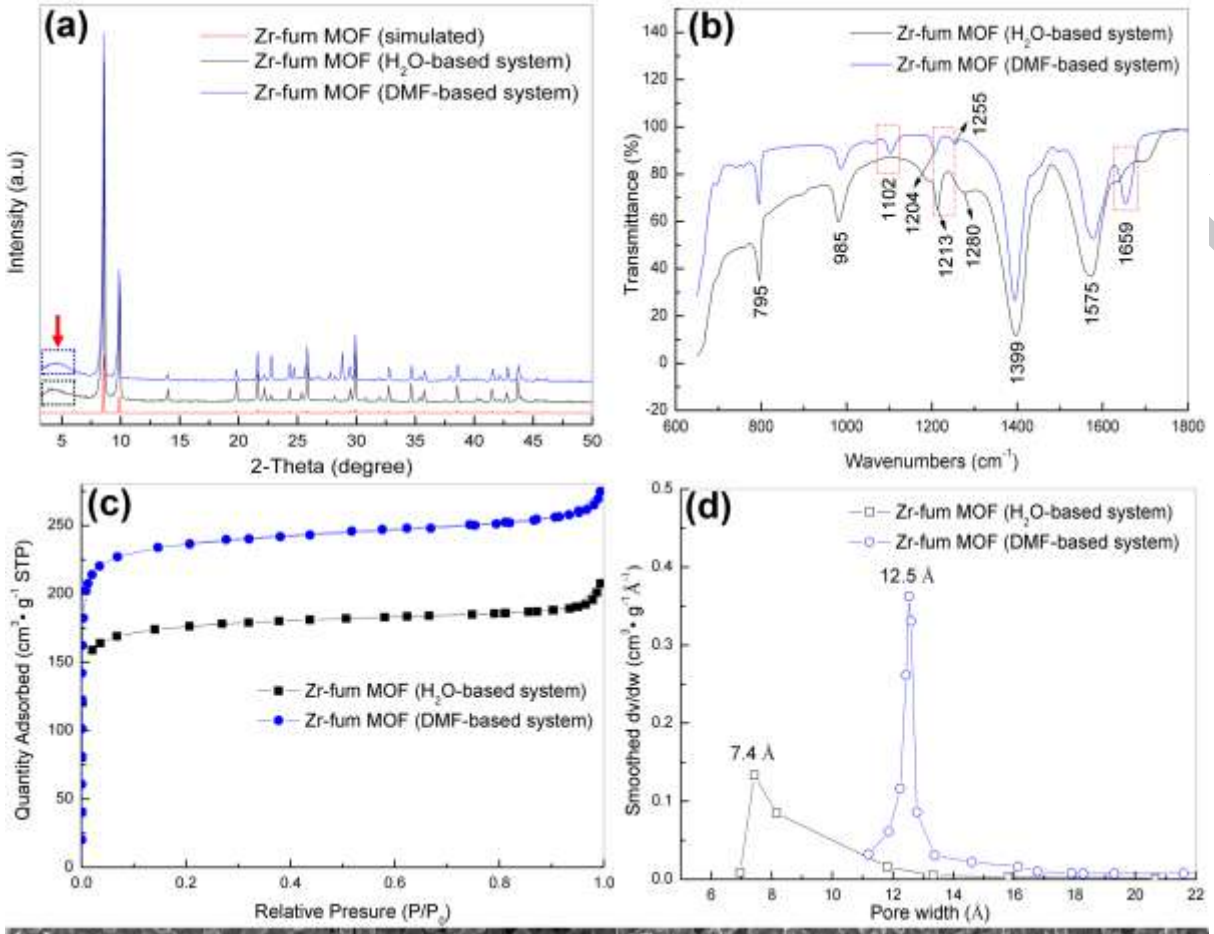

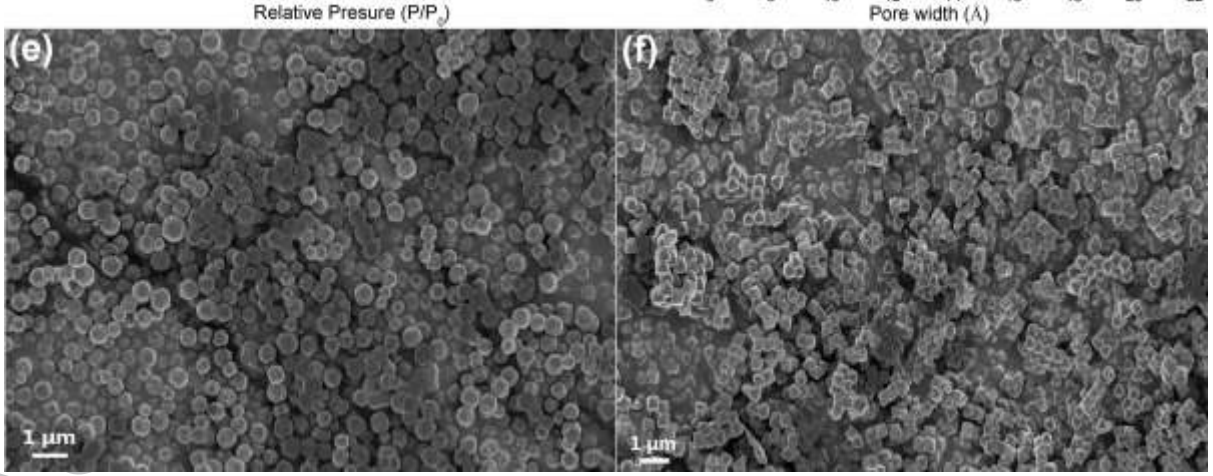

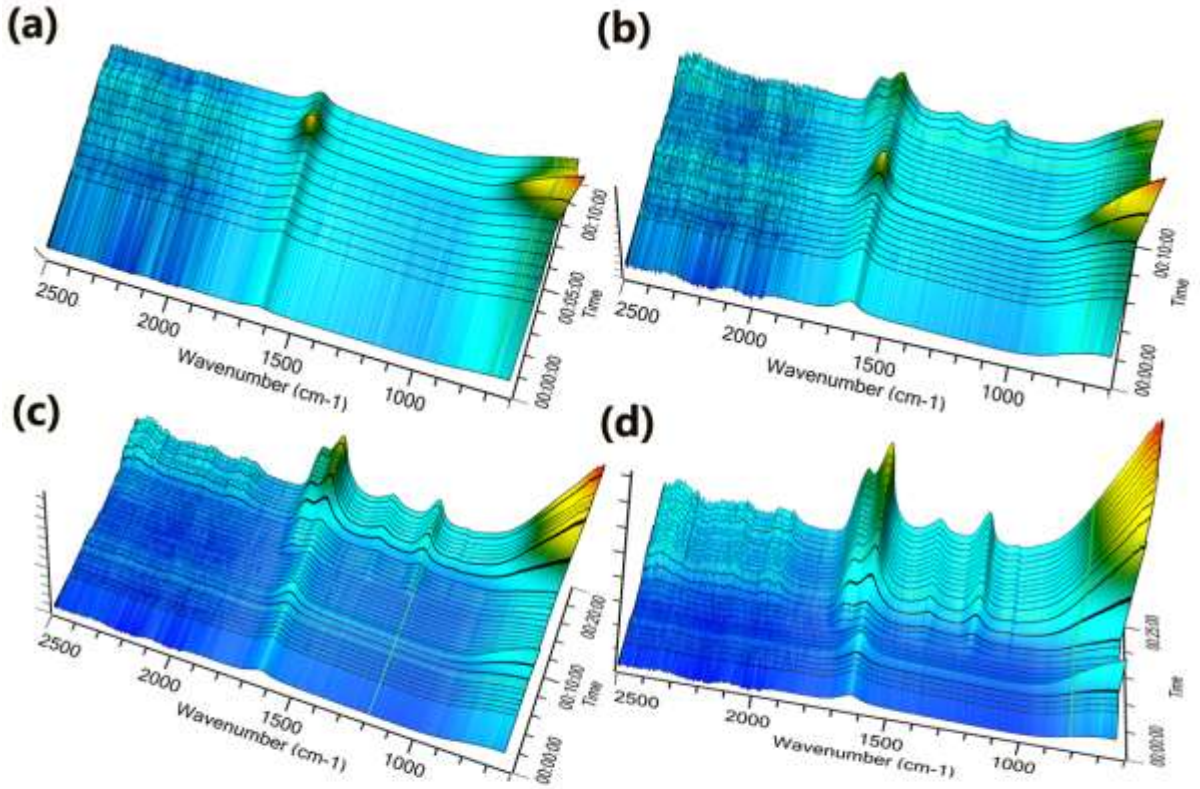

$$1.\ ZrCl_4 + 2.\ C_4H_4O_4 \xrightarrow[4.\ H_2O,\ 80^{\circ}C,\ 20h]{3.\ HCOOH} 5.\ Zr\text{-}fum\ MOF$$

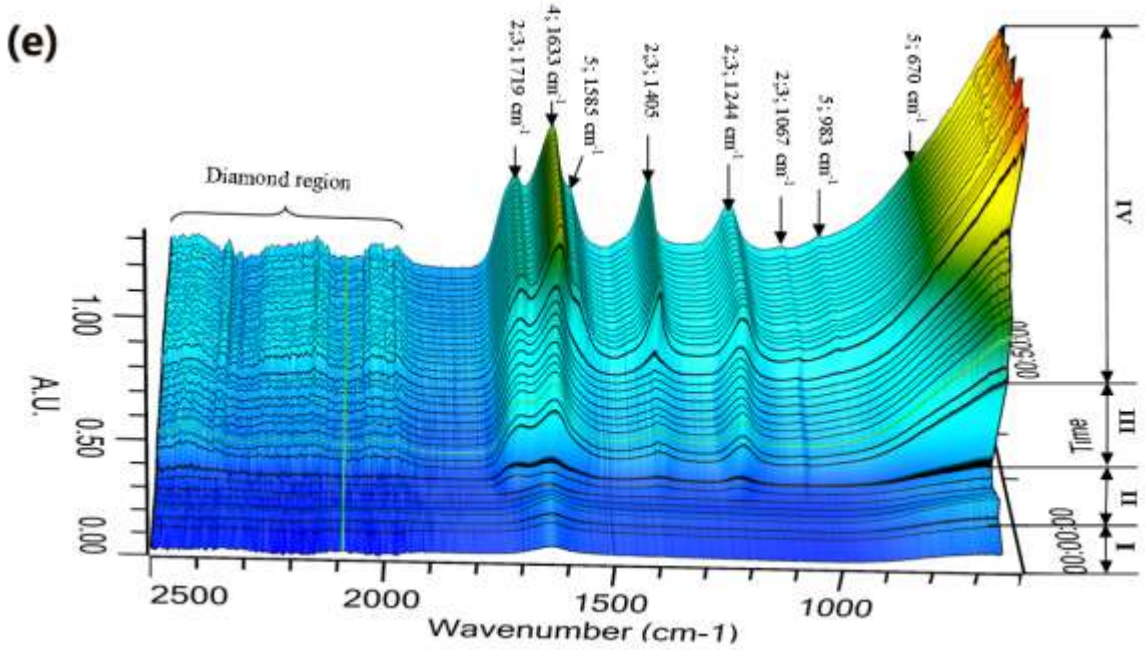

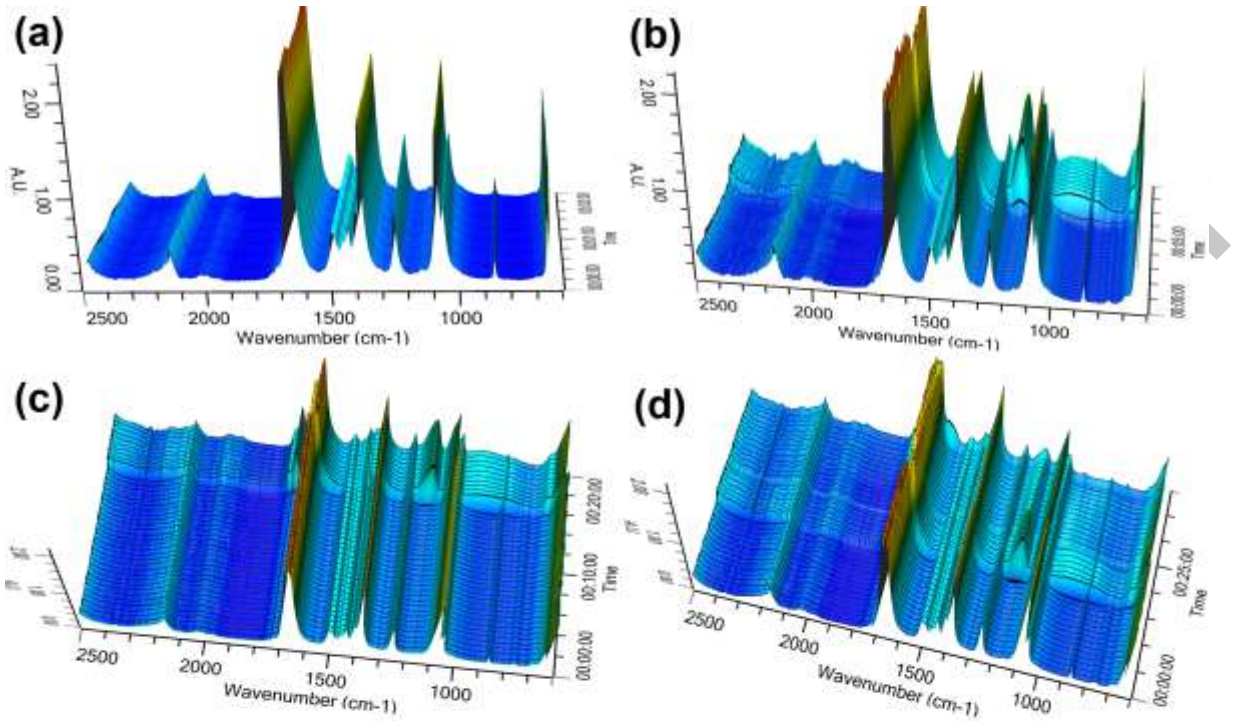

$$1.\ ZrCl_4 + 2.\ C_4H_4O_4 \xrightarrow[4.\ DMF,\ 80\ ^{o}C,\ 20\ h]{3.\ HCOOH} 5.\ Zr-fumMOF$$

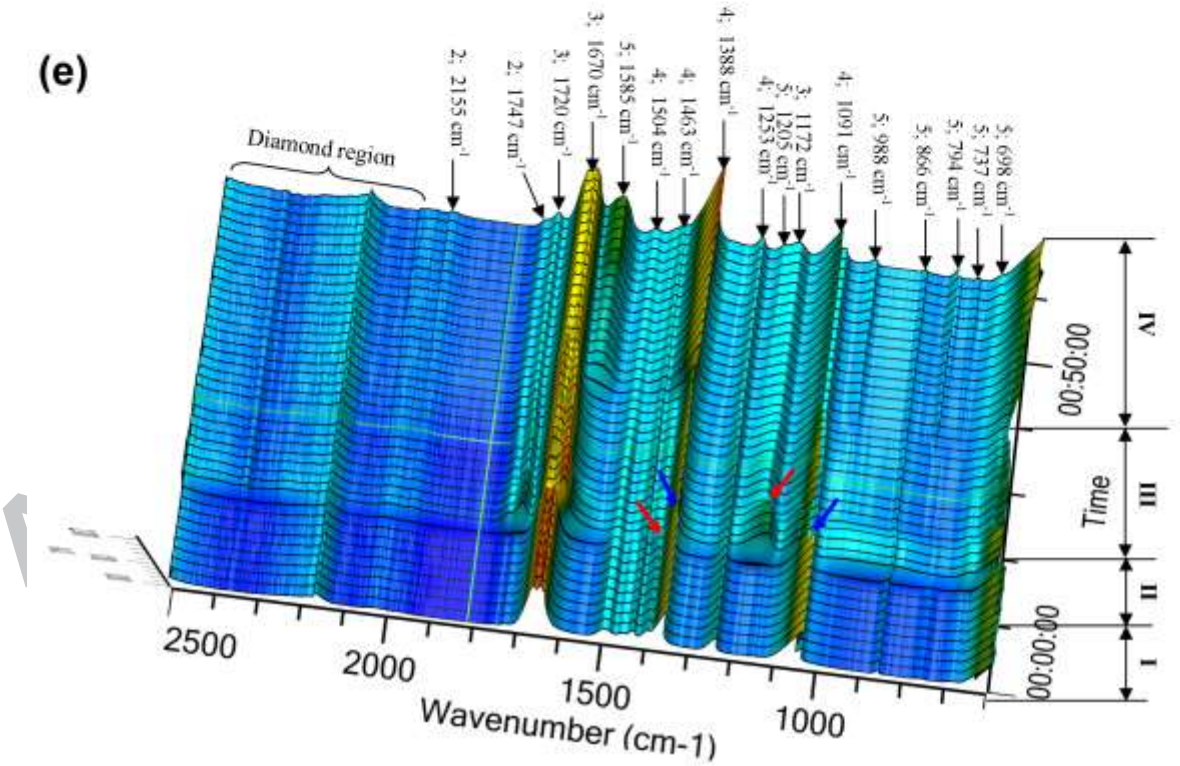

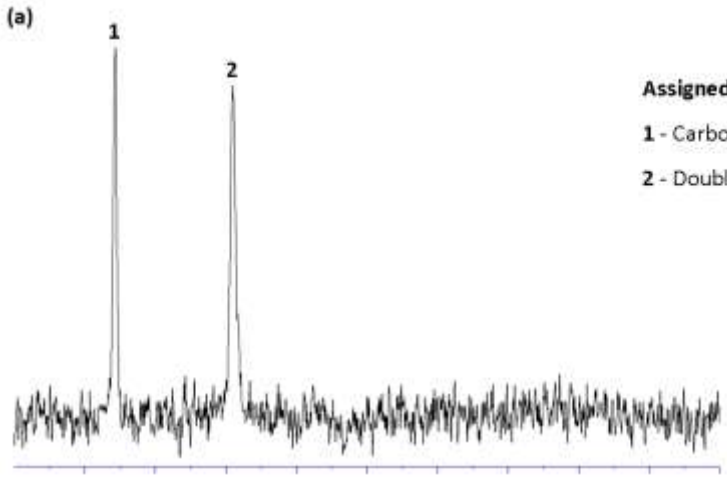
(a)
1
2
Assigned signals:
1 - Carbonyl
2 - Double bond carbon

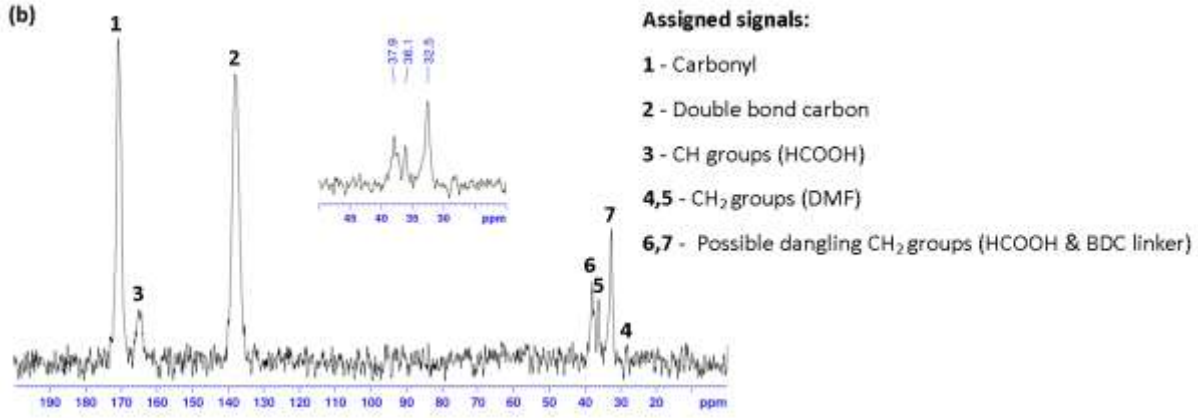
(b)
1
2
3
4
5
6
7
37.9
36.1
32.9
ppm
Assigned signals:
1 - Carbonyl
2 - Double bond carbon
3 - CH groups (HCOOH)
4,5 - CH2 groups (DMF)
6,7 - Possible dangling CH2 groups (HCOOH & BDC linker)